CrossMark

ORIGINAL PAPER

Three-dimensional and immune electron microscopic analysis of the secretory pathway in *Saccharomyces cerevisiae*

Galina V. Beznoussenko[1,2] · Antonella Ragnini-Wilson[2,3] · Cathal Wilson[2,4] ·
Alexander A. Mironov[1,2]

Abstract Until now, the mechanisms of ER-to-Golgi and intra-Golgi transport remain obscure. This is especially evident for the Golgi of *S. cerevisiae* where different Golgi compartments are not organized in stacks. Here, using improved sample preparation protocols, we examined the 3D organization of pre-Golgi and Golgi compartments and found several new features of the structures functioning along the secretory pathway. In the cytoplasmic sheet ER, we found narrow pores that aggregated near the rims, and tubular networks tightly interconnected with sheets of several cytoplasmic ER cisternae. Within the Golgi compartments, we found disks with wide pores, disks with narrow pores, and disk-like networks with varicosities or nodules at the point of branching and thick membranes. Sometimes, these compartments contained 30 nm buds coated with a clathrin-like coat. The lumen of these Golgi compartments was more osmiophilic than the lumen of the ER. In contrast to ER elements, Golgi compartments were isolated and in the majority of cases not connected, although we observed some connections between Golgi compartments and also between Golgi disks with wide pores and the ER. Two types of free vesicles of 35–40 and 45–50 nm were found, the former being sometimes partially coated with a clathrin-like coat. Sec31, a COPII component, was found near narrow pores in the cytoplasmic sheets of the ER, over edge aggregates of narrow pores, and within the ER network. The cis-Golgi marker Rer1p was detected on disks or semi-spheres with wide pores, while the medial Golgi marker Gos1p was found on disks or semi-spheres with narrow pores. Gos1p was found to be enriched on 45–50 nm vesicles, while Rer1p was depleted. The 35–40 nm vesicles did not show either label. These findings are discussed from the point of view of mechanisms of transport.

✉ Alexander A. Mironov
alexandre.mironov@ifom.eu

Galina V. Beznoussenko
galina.beznusenko@ifom.eu

Antonella Ragnini-Wilson
antonella.ragnini@uniroma2.it

Cathal Wilson
wilson@tigem.it

[1] Istituto FIRC di Oncologia Molecolare (IFOM-IEO Campus), Via Adamello 16, 20139 Milan, Italy

[2] Department of Cell Biology and Oncology, Consorzio Mario Negri Sud, Via Nazionale 8/A, 66030 Santa Maria Imbaro, CH, Italy

[3] Department of Biology, University of Rome Tor Vergata, Via della Ricerca Scientifica 1, 00133 Rome, Italy

[4] Telethon Institute of Genetics and Medicine, Via Campi Flegrei, 34, 80078 Pozzuoli, Naples, Italy

Introduction

The Golgi is the central processing and sorting station along the secretory pathway. Newly synthesized proteins destined for secretion or for delivery to different organelles are transported from the endoplasmic reticulum (ER) to the Golgi where they undergo progressive modification by resident Golgi enzymes until they are finally sorted at the trans-Golgi network (TGN).

There is a consensus that in the yeast *S. cerevisiae*, secretory cargo proteins exit the ER from many small ER exit sites (ERES) which appear as numerous small highly dynamic spots over the ER when detected by fluorescently tagged COPII coat proteins (Castillon et al. 2009; Levi et al. 2010; Shindiapina and Barlowe 2010; Okamoto et al. 2012). COPII-coated vesicles enriched in cargo proteins can be isolated from ER microsomes derived from *S. cerevisiae* in the presence of GTP (Barlowe et al. 1994). In permeabilized *S. cerevisiae* cells, COPI- and COPII-coated vesicles bud directly from the ER (Bednarek et al. 1995). However, until now buds have not been described on the ER even when electron microscopy and tomography have been used (Preuss et al. 1991; Morin-Ganet et al. 2000; O'Toole et al. 2002; West et al. 2011; Mari et al. 2014) and it remains unclear whether free, COPII-coated vesicles represent true transport carriers in vivo. Recently, high-speed, high-resolution confocal microscopy showed that the cis-Golgi approaches and contacts the ERES, capturing the cargo as it leaves the ER. Although this does not rule out the possibility of free COPII vesicles, they would be very short-lived and immediately captured by the cis-Golgi (Kurokawa et al. 2014). A similar situation seems to pertain in plant cells (Hawes 2012).

Similarly, there is uncertainty regarding transport mechanisms through the Golgi. Several models of intra-Golgi transport [vesicular, cisternal maturation, diffusion, kiss-and-run (KAR)] to explain intra-Golgi transport compete with each other for the name of the paradigm within the intracellular transport field. The pros and cons of these models have been extensively discussed in Glick and Luini (2011) and Mironov et al. (2013).

In most eukaryotes, the structure of the Golgi is similar being composed of disks organized in stacks, 52 nm spheres localized near stacks, and rarely visible tubules sometimes connecting disks (Polishchuk and Mironov 2004). In *S. cerevisiae*, immunofluorescent detection of different Golgi marker proteins revealed that they form dots that do not overlap with each other (Papanikou and Glick 2009). For instance, Och1p-HA, a cis-Golgi mannosyl-transferase, and Sec7p, a GTPase that is localized within the trans-Golgi, do not co-localize (Rossanese et al. 1999). Golgi membranes are relatively small in size and simple in organization (Preuss et al. 1992; Rambourg et al. 1995).

While the Golgi cisternae in mammalian cells are arranged as stacks that are laterally connected by tubular continuities to form a ribbon (Polishchuk et al. 1999; Mironov et al. 2013), this is not the case in *S. cerevisiae* where the Golgi compartments are dispersed. Rambourg et al. (1993, 1995, 2001) described three different types of the Golgi compartments: (i) a planar membrane or bent disks with different numbers of narrow perforations; (ii) spherical or plane networks with many perforations and the absence of nodules; (iii) networks with nodular varicosities in their branching points. These structures had diameters that were not more than 900 nm. Recently, the three-dimensional organization of the *cis*-Golgi in *S. cerevisiae* was examined with the help of electron microscopic tomography (Mari et al. 2014), where the authors observed cylindrical conformations with fenestrations and vesicle budding and/or fusion profiles on both the internal and external surfaces. Recent 3D reconstruction of the yeast Golgi also did not show COPI-coated buds on the Golgi (Papanikou et al. 2015). Analysis of 8 movies containing 3D EM of yeast cells described by West et al. (2011) revealed the following types of Golgi in S. cerevisiae: disks (87 %), invaginated disks (10 %), and small 3D networks (3 %). Single-membrane cisternae rarely showed buds or vesicle fusion profiles. Finally, possible direct contact between different Golgi compartments visible at the level of light microscopy has been reported (Matsuura-Tokita et al. 2006; Nakano and Luini 2010).

Being isolated from each other, disk-like or tubular network-like Golgi structures are often similar to membranes of the ER (Preuss et al. 1991; West et al. 2011). This makes the discrimination of sections that pass through the Golgi and the ER rather difficult. Therefore, several criteria have been proposed for their discrimination: (i) ER cisternae are always connected with each other, Golgi cisternae are isolated from each other; (ii) ER cisternal perforations are wider than perforations of the Golgi disks; (iii) ER cisternae are longer than Golgi disks, semi-spheres or networks, and are always connected with another part of the ER; (iv) the lumen of the Golgi compartment contains more dense content than that of the ER [glycosylated material that stains positively with reduced osmium (Rambourg et al. 1995; West et al. 2011)]. Finally, the identification of the rough ER can be based on the presence of ribosomes (West et al. 2011).

Here, we examined the three-dimensional organization of the yeast Golgi using new methods of sample preparation for electron microscopy (EM) designed for the visualization of yeast membranes and found rare connections between different Golgi compartments when these compartments are in close apposition to each other. The ER of yeast cells does not exhibit any bud-like profiles, whereas Golgi compartments contained rather few bud-like profiles. We found two types of isolated vesicles (with <40 or 52 nm in diameter) in the cytosol. These data are discussed from the point of view of different models of intracellular transport.

Materials and methods

Yeast strains and plasmids

The plasmid expressing GFP-tagged Rer1p was kindly provided by A. Nakano (The University of Tokyo. Tokyo.

Japan; described in Sato et al. 2001). The plasmid expressing GFP-tagged Gos1p was constructed by amplifying the ORF from genomic DNA and cloning in the vector pUG36. The RFP-tagged Gos1p construct was obtained by replacing the GFP gene in pUG34 with monomeric RFP and then cloning in the GOS1 gene. Yeast cells (strain BY4742) were transformed with these constructs using standard protocols.

Antibodies

We used a commercially available goat polyclonal antibody against Sec31p from *S. cerevisiae* (yC-20) from Santa Cruz Biotechnology (Heidelberg, Germany). For transformed cells, we used polyclonal anti-GFP antibody (ab6556) from Abcam (Cambridge, UK).

Fluorescence microscopy

Strains expressing GFP-tagged proteins were grown to log phase in selective minimal media and observed directly. Cells were viewed using a Nikon Eclipse TE2000-U microscope equipped with HBO 100-W UV lamp (OSRAM), cooled color camera DS-5Mc-U1 (Crisel Instruments), high-speed filter wheel system (Crisel Instruments) controlled by the MetaMorph software (MetaImage Series 7.0, Molecular Devices). Image processing was performed with Photo-Shop 8.0.1 (Adobe Systems).

Cryo-immuno-electron microscopy

Cryo-immune-EM was performed as described (Vanhecke et al. 2007) using the transformed *S. cerevisiae* cells grown to mid-log phase. The GFP-tagged versions of Rer1p and Gos1p were detected in the immune-EM using the polyclonal anti-GFP antibody diluted 1:250.

Routine electron microscopy

For routine electron microscopy (Kolpakov et al. 1996), cells were fixed with 1 % glutaraldehyde in HEPES (pH 7.0), post-fixed in reduced OsO_4 for 2 h, washed, treated with 0.3 % thiocarbohydrazide for 30 min and then, after the washout, with 1 % OsO_4 for 1 h (sometimes treatment with thiocarbohydrazide and OsO_4 was made three times) following dehydration and embedding in Epon-812. The OTOTO methods were applied as described (Ryan and Hart 1986). Only cells with a bud sectioned in parallel to their long axis were examined.

High-pressure freezing

High-pressure freezing (HPF) was performed using a Bal-Tec HPM010 high-pressure freezer (Bal-Tec AG,

Principality of Liechtenstein) and using interlocking brass hats as the specimen carrier (Swiss Precision Inc., Palo Alto, CA, USA). Cells were harvested, centrifuged, and inserted into cellulose microcapillaries (Leica Microsystems, Vienna). We used cellulose capillaries for HPF of yeast cells according to Hohenberg et al. (1994). Briefly, the cell suspension was centrifuged briefly and the pellet was diluted twofold. Then, short tubes from cellulose (Leica AFS; Leica Microsystems, Vienna) with an internal diameter of 200 nm were soaked in the bottom of the test tube. Capillary forces elevated the cell suspension into the cellulose tube. The ends of the cellulose tubes were closed with the help of forceps and placed into the HPF holder from Leica. The carriers were placed in the freezer and subjected to HPF. Subsequently, freeze substitution (FS) was performed using an automatic FS unit (Leica AFS; Leica Microsystems, Vienna) with 4 % OsO_4 in 95 % acetone in 1.5-ml conical Eppendorf centrifuge tubes (Eppendorf UK Ltd., Cambridge, UK). In several cases, samples were rehydrated using acetone with increasing concentrations of water and then samples were treated with the OTOTO procedure as described above. Samples were then subjected to 24-h treatment with 0.1 % OsO_4 and only then water was eliminated using solutions of increasing concentrations of ethanol and then embedded in Epon (Beznoussenko and Mironov 2015).

The slightly modified high-pressure-freezing and freeze-substitution protocol was based on the use of a 4 % OsO_4 solution in 95 % acetone (Walther and Ziegler 2002). This included the following additional steps: Samples were treated with mixtures of acetone and water where the concentration of water was increased gradually. Then, samples were treated with 0.3 % thiocarbohydrazide for 20 min, washed, and then treated with 1 % OsO_4 for 20 min. The cells were dehydrated in ethanol and embedded into Epon 812 and polymerized at 60 °C. In order to prevent shrinkage of samples during tomographic analysis, we used a methyl nadic anhydride (MNA)-based Epon 812 hard resin (Luft 1961). This resin appeared to be the most resistant to the electron beam (Kreft et al. 2010; Micaroni et al. 2010). Our methods of sample preparation allow the examination of sections without contrasting of samples with uranyl acetate and lead citrate. It improved the quality of the EM images of membranes allowing the visualization of thin tubules in yeast cells.

Tomography

An ultratome (Leica AFS; Leica Microsystems, Vienna) was used to cut 60 nm serial thin sections and 200 nm serial semi-thick sections. Sections were collected onto 1 % Formvar films adhered to slot grids. Both sides of the grids were labeled with fiduciary 10 nm colloidal gold (British
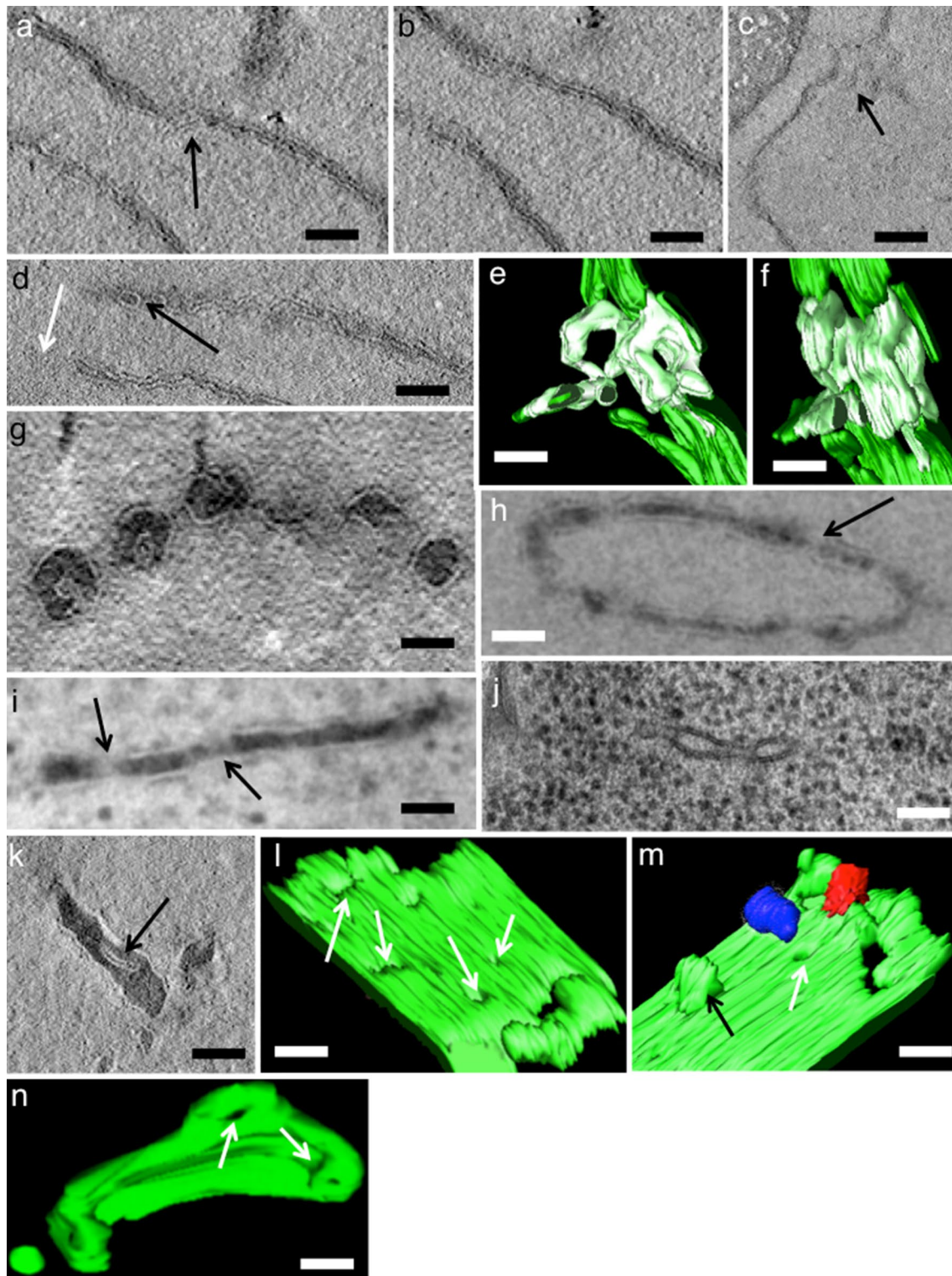
Biocell International). Tilt series were collected from the
samples from ±65° with 1° increments at 120 or 200 kV
in Tecnai 12 or Tecnai 20 electron microscopes (FEI, Ein-
dhoven. the Netherlands) as described previously (Mironov
et al. 2004; Beznoussenko et al. 2007).

Tilt series were recorded at a magnification of 20,000 × or
60,000 × using software supplied by the instrument. The
nominal resolution in our tomograms was 4 nm, based
upon section thickness, the number of tilts, tilt incre-
ments, and tilt angle range (Koster et al. 1997). The IMOD

◄**Fig. 1** Secretory pathway structures in *S. cerevisiae* cells revealed using the OTO (mostly) and OTOTO methods and 2-step image acquisition. **a–f** Membranes of the ER and ERES. Lipid membranes appear as structures composed of three layers (*dark, light, dark*). The *arrow* in **a** shows a pore in the sheet of cytoplasmic ER. **b** A serial virtual section is presented where the pore is no longer observed. The *thin arrow* in **d** shows the edge accumulation of narrow pores. The *white arrow* indicates a nuclear pore. **c** A virtual section of the ER network taken from the section c10 in Fig. S1 (*white box*). The *arrow* indicates a COPII-like coat at the edge of an ER network. This second tomogram was obtained at a magnification of 29,000 after examination of the set of primary tomograms shown in Fig. S1 and selection of area within *white dashed box* in Fig. S1c10. A 3D model of this network is shown in **e, f. g** OTOTO method. A disk with wide pores. **h** Routine section of a spherical type of compartment with wide pores (*arrow*). **i** Routine section of a disk with narrow pores (*arrows*, OTO protocol). **j** A disk with narrow pores after high-pressure freezing and cryo-substitution. **k** A tangential virtual section of a disk with narrow pores (*arrow*). **l, m** A 3D model of the disk with narrow pores (*white arrows*) shown from two sides. *Green* protrusion in (**m**, *black arrow*) indicates COPI-dependent bud, whereas *red* and *blue* spheres show COPI-dependent vesicles. **n**, a disk with narrow pores (*white arrows*) forming a structure similar to a deflated ball. *Scale bars* 60 nm panels **a, b, d–f, g, k–n**; 200 nm panel **c**; 130 nm panels **h–j**

package (Kremer et al. 1996; Mastronarde 2005) and its newest viewer, 3DMOD 4.0.11, were used to construct individual tomograms and for the assignment of the outer leaflet of organelle membrane contours, and best-fit sphere models of the outer leaflet were used for vesicle measurements (Mironov and Mironov 1998; Polishchuk et al. 1999; Weigert et al. 1997; O'Toole et al. 2002). Videos were made in 3DMOD and assembled in QuickTime Pro 7.5 (Apple), and the video size was reduced to <10 MB by saving videos as an HD 720p in QuickTime. Out of a total of 31 tomograms examined, 16 were from samples where two Golgi compartments that were different in shape were situated close to each other.

Estimation of labeling density and other morphometric parameters was performed according to Mironov and Mironov (1998) and Mayhew and Lucocq (2008). Sometimes it was difficult to distinguish a cis-Golgi compartment from a trans one. Discrimination of cis- and trans-Golgi compartments was performed on cryo-sections. The thickness of membranes was significantly higher on trans-Golgi compartments than on cis.

Correlative light-electron microscopy

Log phase yeast cells transformed with a plasmid expressing GFP-Rer1p were plated on concanavalin-coated MatTek grided plates, observed by fluorescent microscopy and then fixed briefly (2 min) with 0.1 M HEPES pH 7.2, 0.2 % glutaraldehyde, washed three times with water, and fluorescent images were acquired at the microscope. After acquisition, the cells were covered with a thin layer of 2 % gelatin and processed for electron microscopy.

Results

Improved methodologies for visualizing membranes in yeast

Establishing continuity or discontinuity of structures requires a high level of resolution. High concentrations of proteins in the cytosol, their high affinity for OsO_4, and low levels of Os precipitation on yeast membranes impede electron microscopic analysis of yeast cells. Post-fixation and contrasting with $KMnO_4$ (Baharaeen and Vishniac 1982; Preuss et al. 1992; Rambourg et al. 1993; Wright 2000); quick-freezing-cryo-substitution (Kang and Staehelin 2008); fixation with reduced OsO_4 (Rambourg et al. 1993; Morin-Ganet et al. 2000); embedding in epoxy (Rambourg et al. 1995, 2001) or acrylic (Banta et al. 1988; O'Toole et al. 2002; West et al. 2011; Okamoto et al. 2012; Kukulski et al. 2011, 2012a, b) resins; and cryo-sectioning (Preuss et al. 1992) in combination with EM tomography of Tokuyasu cryo-sections (Mari et al. 2014) have been used for the EM analysis of *S. cerevisiae*. However, application of all of these EM methods did not enable us to visualize thin membrane tubules, especially in 3D. In order to improve the EM resolution, we used three new approaches: (1) new fixation/contrasting/embedding protocols, modifying the OTO and OTOTO methods (Geissinger et al. 1983; Ryan and Hart 1986) and applying a high-pressure-freezing and freeze-substitution protocol based on the use of a 4 % OsO_4 solution in 95 % acetone (Walther and Ziegler 2002); (2) a new method of image acquisition with tomographic acquisition of images from random or serial 150–200 sections and when we found some important phenomenon, we repeated tomography acquisition at a higher magnification; (3) immune-EM labeling combined with CLEM and quantitative analysis. The resolution of our images along the *X-*, *Y-*, and *Z*-axes was 3 nm. After cryo-substitution, ribosomes were better visualized than after the OTO method.

Initially, we performed random or serial tomographic reconstructions at a magnification of 12,000 (Fig. S1c). Then, after analysis of tomograms, we acquired tomograms at a higher magnification (29,000 or more; Fig. 1c, e, f; S1c10 [white box]). Visualization of membranes was significantly improved (Figs. 1, 2, S1, S2). The membranes of the cristae of mitochondria were well visible (Fig. S1a, arrow).

Secretory pathway structures in *S. cerevisiae*

We found four different domains within the ER, namely nuclear envelope, cytoplasmic sheets of the ER (Fig. 1a–d), the ER attached to the PM, and tubular ER localizing mostly within cell bud, as also described by West et al. (2011). Our sequential tomography approach allowed us to

visualize not only wide pores in the cytoplasmic ER sheets (Fig. 1a), but also small pores with a diameter of 40 nm and their aggregation near the rims of cytoplasmic sheets (Fig. 1d: thin arrow; Fig. S3 g: arrow). We also found tubular networks with narrow pores localized at sites where several rims of cytoplasmic sheets with an aggregation of narrow pores near the rims contacted each other (Fig. 1c, e, f, see also S1c10 [white dashed box] and full reconstruction in Fig. S5a). We found some COPII-like coats on these membranes at the edges of ER networks (Fig. 1c, arrow). However, we could not identify any COPII-coated buds.

We found three types of Golgi compartments: (1) disks with wide pores (Fig. 1g; Fig. S3a, b, c, f: black arrow); (2) disks with narrow pores (Fig. 1i–n; S3b, white arrow; d, e: black arrows; S3f: black arrow); and (3) disks with wide pores and nodules at the points of branching (Fig. 2a–f; S3b: black arrow). In these last compartments, we observed 35 nm buds with a clathrin-like coat (Fig. 2d, e). The number of pores in disks with wide pores was 6 ± 2; the number of pores in disks with narrow pores was 5.5 ± 1.7. About 2–3 % of Golgi compartments with wide and narrow pores exhibited the shape of a deflated ball (Fig. S3e), which on sections showed the shape of perforated spheres. Golgi compartments differed from ER elements by their isolated nature and the more dense contents of the lumen. After quick-freezing cryo-substitution, we found similar Golgi structures (Fig. S2). Blind calculation of 257 Golgi compartments revealed that 22 % of them were disks with wide pores and thin membranes, 33 % were disks with narrow pores, and 45 % were disks with varicosities, wide pores, and thick membranes. We did not perform 3D reconstruction of the ER and Golgi disks with wide pores, which has been performed excellently by West et al. (2011).

Two types of free (isolated) vesicles were found in the cytoplasm with a diameter of 35–40 nm (average diameter 37 ± 1.6) (Fig. 2i, j; Fig. S5b: red spheres) and 45–50 nm (average diameter 47 ± 3.9) (Fig. 2g, h; Fig. S5b, orange spheres). Secretory granules were usual (Fig. 2f; Figs. S3 h, S5b pictured in blue). The number of 45–50 nm vesicles was 4.6 ± 0.7-fold higher than the number of 35–40 nm vesicles (Fig. S5b). We found two 37 nm vesicles partially coated with a clathrin-like coat (Fig. 2j), the thickness of the coat being about 18 nm and containing T-spikes. We did not observe any 60–70 nm vesicles near the ERES.

Immune-EM of COPII and Golgi markers

An antibody against Sec31p, a component of the COPII complex, labeled narrow pores in the sheets of the cytoplasmic ER and aggregations of pores near the ER rims (Fig. 3a–e). Sec31p was also present within tubular networks highly connected with several sheets of cytoplasmic ER (Fig. 3c, f). There was no labeling for Sec31p

over secretory granules (Fig. 3d) or Golgi compartments (Fig. 3g, h, i).

To identify the shape of two different Golgi compartments, cells were transformed with plasmid constructs encoding GFP-tagged versions of Rer1p and Gos1p that represent the cis and medial Golgi compartments, respectively. Rer1p, a receptor protein required for the retrieval of various endoplasmic reticulum (ER) membrane proteins, cycles between the ER and the Golgi but under steady-state conditions localizes principally on the cis-Golgi (Sato et al. 2001). Gos1p is a SNARE protein that localizes to the medial Golgi (McNew et al. 1998; Matsuura-Tokita et al. 2006). Standard immunofluorescence analysis of these compartments was difficult because good antibodies against compartment markers that work at the electron microscopy level were not available. Fluorescence microscopy of transformed yeast cells showed that both tagged proteins exhibit a typical punctate pattern (Fig. 4a–c), while co-expression of GFP-Rer1p with an RFP-tagged version of Gos1p (RFP-Gos1p) showed that there is no overlap between the two markers, suggesting that they are concentrated in separate Golgi compartments (Fig. 4d; Matsuura-Tokita et al. 2006).

GFP-Rer1p labeled disks with wide pores (Fig. 3j–m) and was present in a few perforated spheres and tubular networks composed of rather smooth tubules (Fig. 4e). The labeling was less intense over tubular networks composed of varicose tubules and over profiles of disks (Fig. 4e, f). In contrast, the medial compartment marker GFP-Gos1p labeled other structures (Fig. 3n, o; S4), which mostly appeared as disks with narrow pores (Fig. 4e, double arrow; 4g, thick arrow) or, rarely, tubular networks composed of tubules with varicosities (Fig. 4e, thick arrow). The 50 nm vesicles were not labeled for GFP-Rer1p, but were enriched in GFP-Gos1p (Fig. S4f, i; Table S1). The 35–40 nm vesicles did not show either label. Additionally, for identification of the cis-Golgi compartment, we used correlative light-electron microscopy (CLEM) and observed that the cis-Golgi, which was labeled with GFP-Rer1p, appeared as tubular networks or highly perforated planes (with wide pores) or invaginated bent disks similar to the shape of a semi-sphere (Fig. S6).

Connections between different Golgi compartments

It was also possible to detect connections between different Golgi compartments, although only when the resolution of the images was high. In 45 tomograms examined (tomograms where two Golgi compartments with different shapes were situated near each other), we found 16 connections (Fig. 5a–e: thin arrows). The new methods allowed us to discriminate connections (Fig. 5a, c, e) from membrane contacts (Fig. 5f, g). The following types of connection were observed: ERES connected with cis-Golgi, cis-Golgi with medial Golgi, medial Golgi with trans-Golgi.
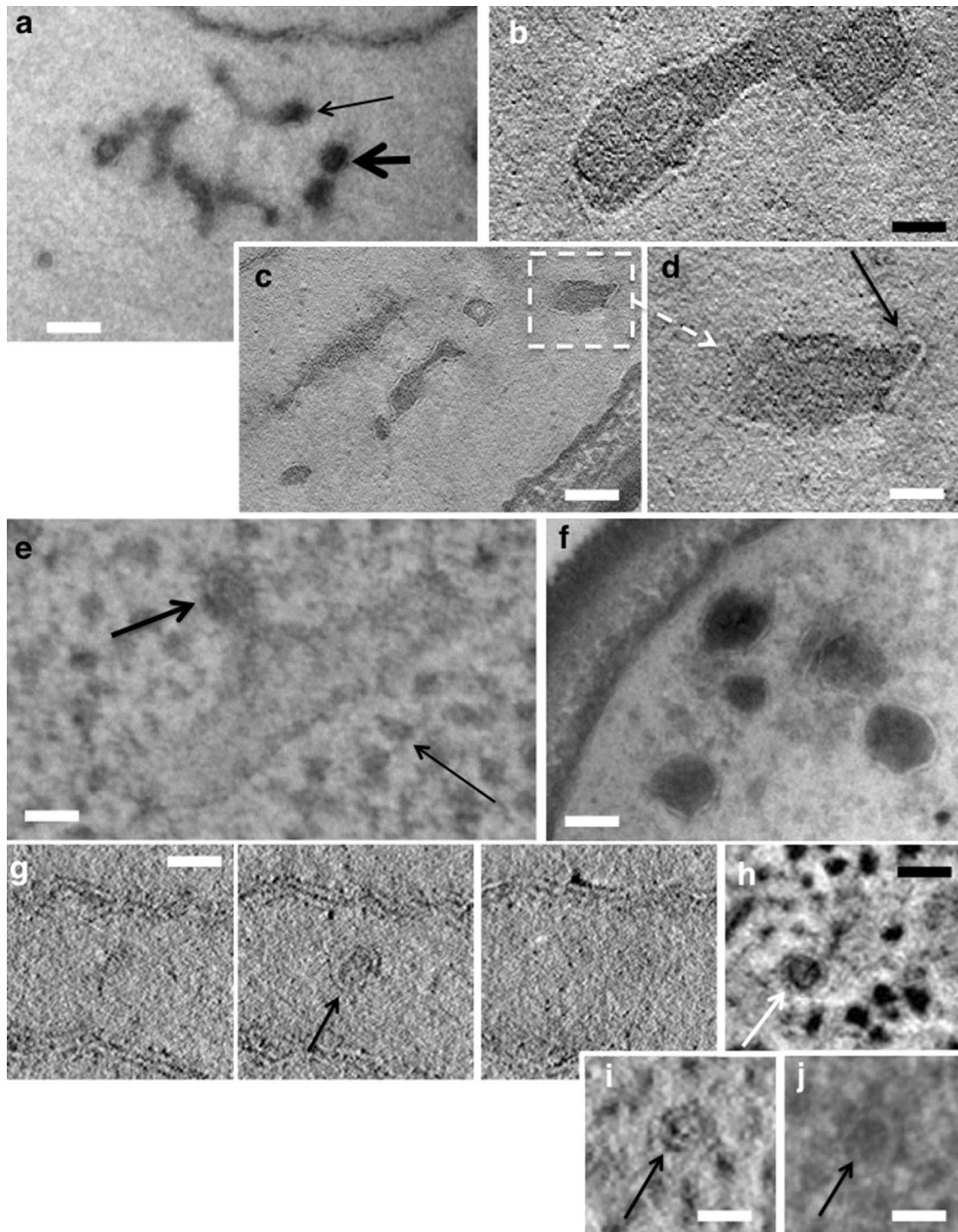
Fig. 2 Structure of trans-Golgi compartments and vesicles. **a** The *thick arrow* shows a secretory granule in the process forming from the presumably trans-Golgi compartment with nodular structures within the branching points. The *thin arrow* indicates a bud, from which a secretory granule is forming. **b** A virtual section from a tomogram. The structure of presumably trans-Golgi elements at higher magnification. **c, d** A clathrin-like coat on a 40 nm bud (**d** higher magnification of the area inside the *white box* in **c**). **e** Routine electron microscopic section of frozen-cryo-substituted cells showing a clathrin-like coat (*thick arrow*) on a 40 nm bud of the trans-Golgi. The *thin arrow* shows ribosomes. **f** Secretory granules with a diameter of about 100 nm surrounded by a trilaminar membrane. **g–j** Different types of vesicles. **g** A 50 nm vesicle (*arrow*) in virtual serial sections showing the absence of the vesicle (*left panel*), the appearance of the vesicle (*middle panel*) and its disappearance (*right panel*). **h–j** 37 nm vesicles (*arrows*); **j** the vesicle is partially coated with a coat containing spikes. *Scale bars* 80 nm panels **a–d**; 60 nm panels **d–f**; 50 nm panels **g–j**
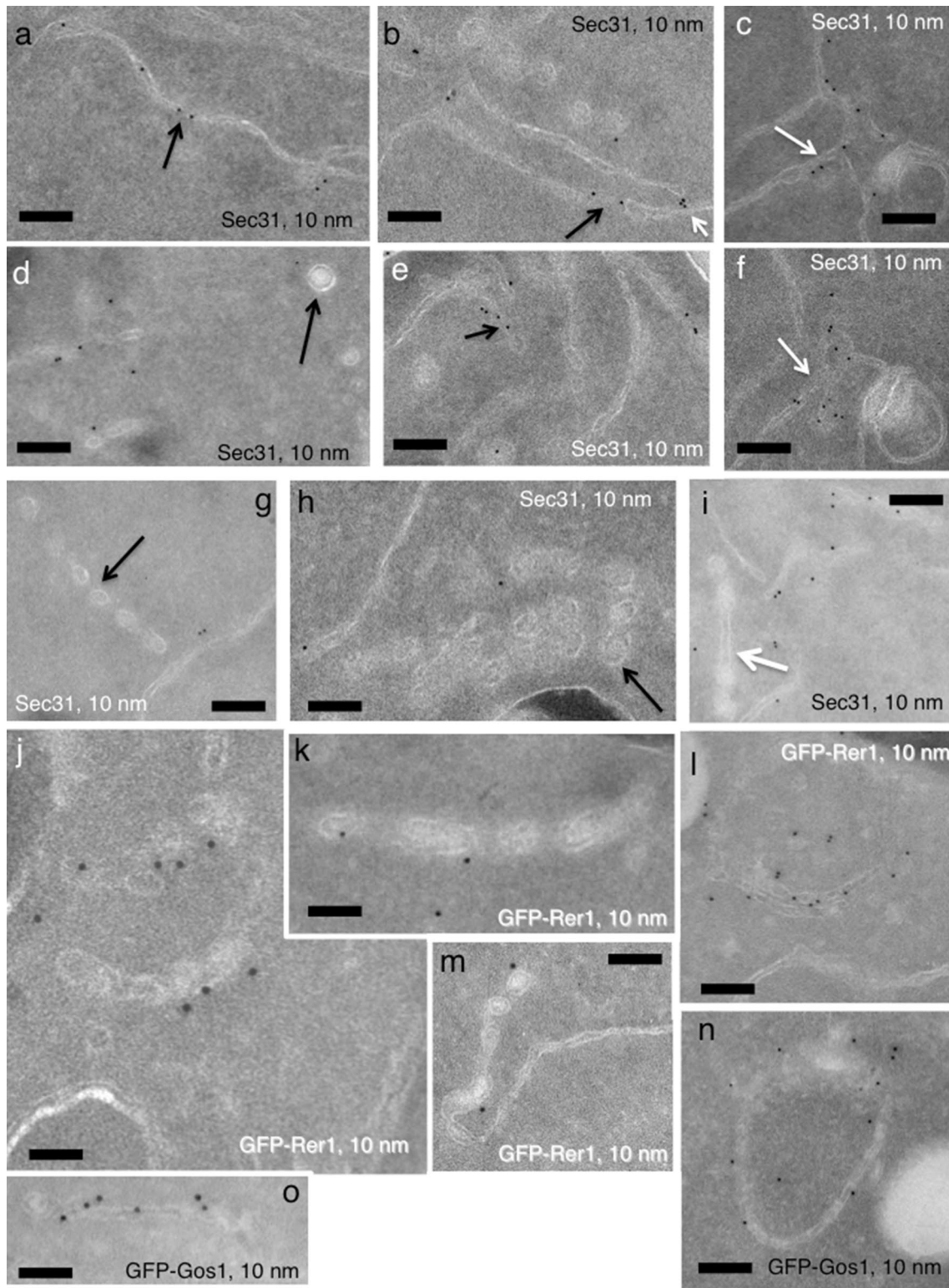
Fig. 3 Immune-EM labeling for Sec31p, GFP-Rer1p, and GFP-Gos1p showing 10 nm *gold particles* which indicate localization of the anti-Sec31 antibody or an anti-GFP antibody for GFP-Rer1p and GFP-Gos1p. **a, b** Sec31p is present around narrow pores (*black arrows*) of the cytoplasmic ER. The *white arrow* in **b** indicates labeling of the pore situated near the branching of the cytoplasmic ER. **c, f** Serial sections showing labeling for Sec31p over the ER network. **d, e** Sec31p labeling over ER edge networks and other structures. The *arrow* in **d** shows a secre-tory granule that does not contain Sec31p labeling. **e** Labeling for Sec31p over edge aggregates of pores (*arrow*). **g–i** No Sec31p labeling was observed on Golgi compartments. The *arrows* indicate the presumably cis-Golgi compartment in **g**, the presumably trans-Golgi compartment in **h**, and the presumably medial Golgi compartment in **i**. **j–o** Immune-EM of cells expressing GFP-Rer1p **j–m** or GFP-Gos1p **n, o**. *Scale bars* 150 nm panels **a–f**; **i**, **l**, **n**; 60 nm panels **h**, **j**; 75 nm panels **g**, **k**, **m**, **o**
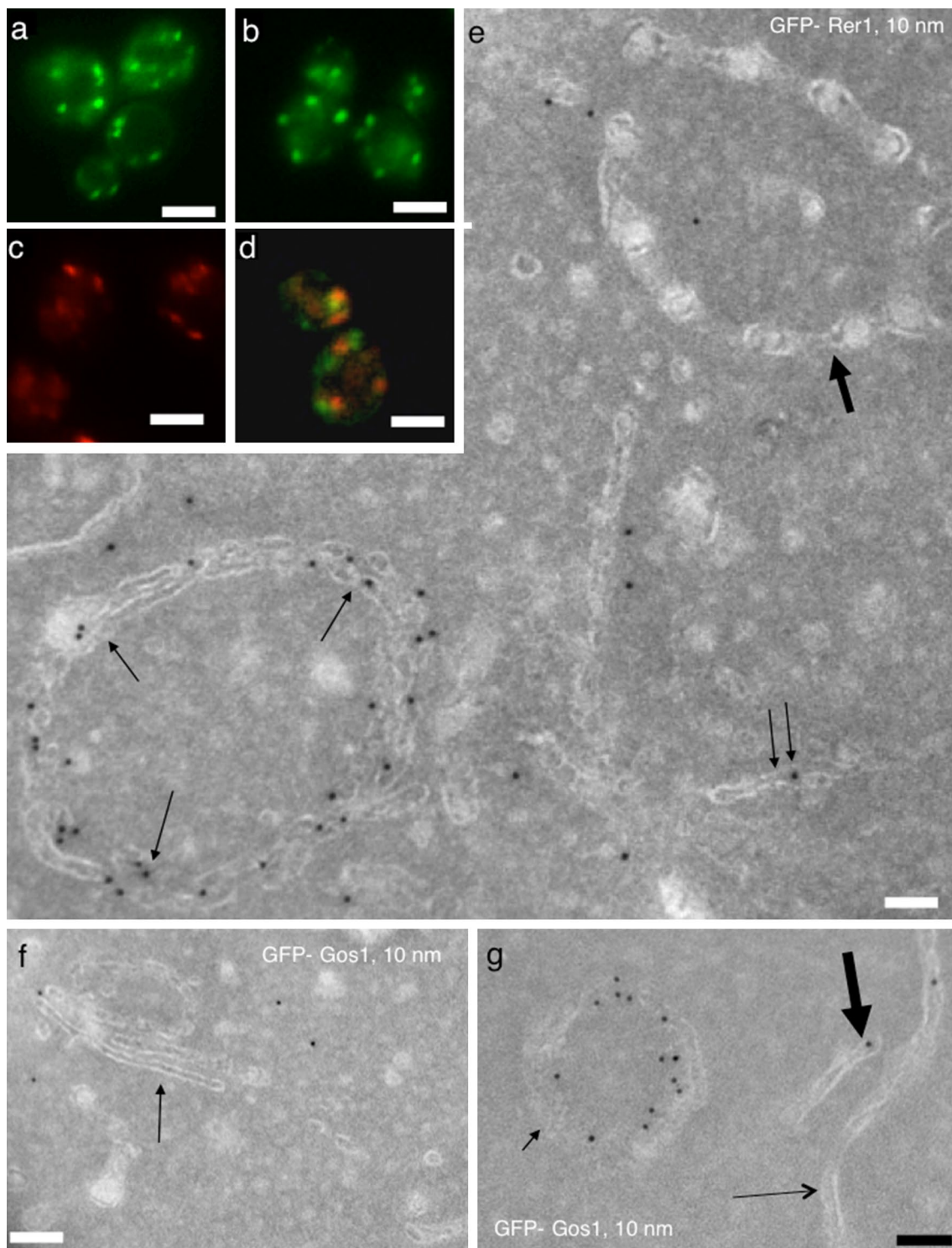
Fig. 4 Localization of cis and medial markers within Golgi compartments. Fluorescence microscopy of yeast cells expressing GFP-Rer1p **a**, GFP-Gos1p **b**, RFP-Gos1p **c**, or both GFP-Rer1p and RFP-Gos1p **d**. Cells expressing GFP-Rer1p or GFP-Gos1p were prepared for cryo-immune-EM and stained with an anti-GFP antibody (**e**−**g**). **e** GFP-Rer1p is visible over perforated ring-like structures composed of rather smooth tubules (*thin arrows*) but not over tubular networks composed of varicose tubules and buds with thick membranes (*thick arrow*). Elongated flat structures without perforations are poorly labeled (*double arrow*). **f**, **g** GFP-Gos1p is present over ring-like structures without perforations (*small arrow* in **g**), but the labeling density was lower over elongated (presumably disk-like structures, *thick arrow* in **g**) and stacked Golgi without a significant number of perforations (*arrow* in **f**). There is little labeling on the ER (long arrow, **g**). No labeling is visible over the trans-Golgi (as in **e**; *thick arrow*). *Scale bars* 3 μm panels **a**–**d**; 62 nm panel **e**; 75 nm panels **f**, **g**
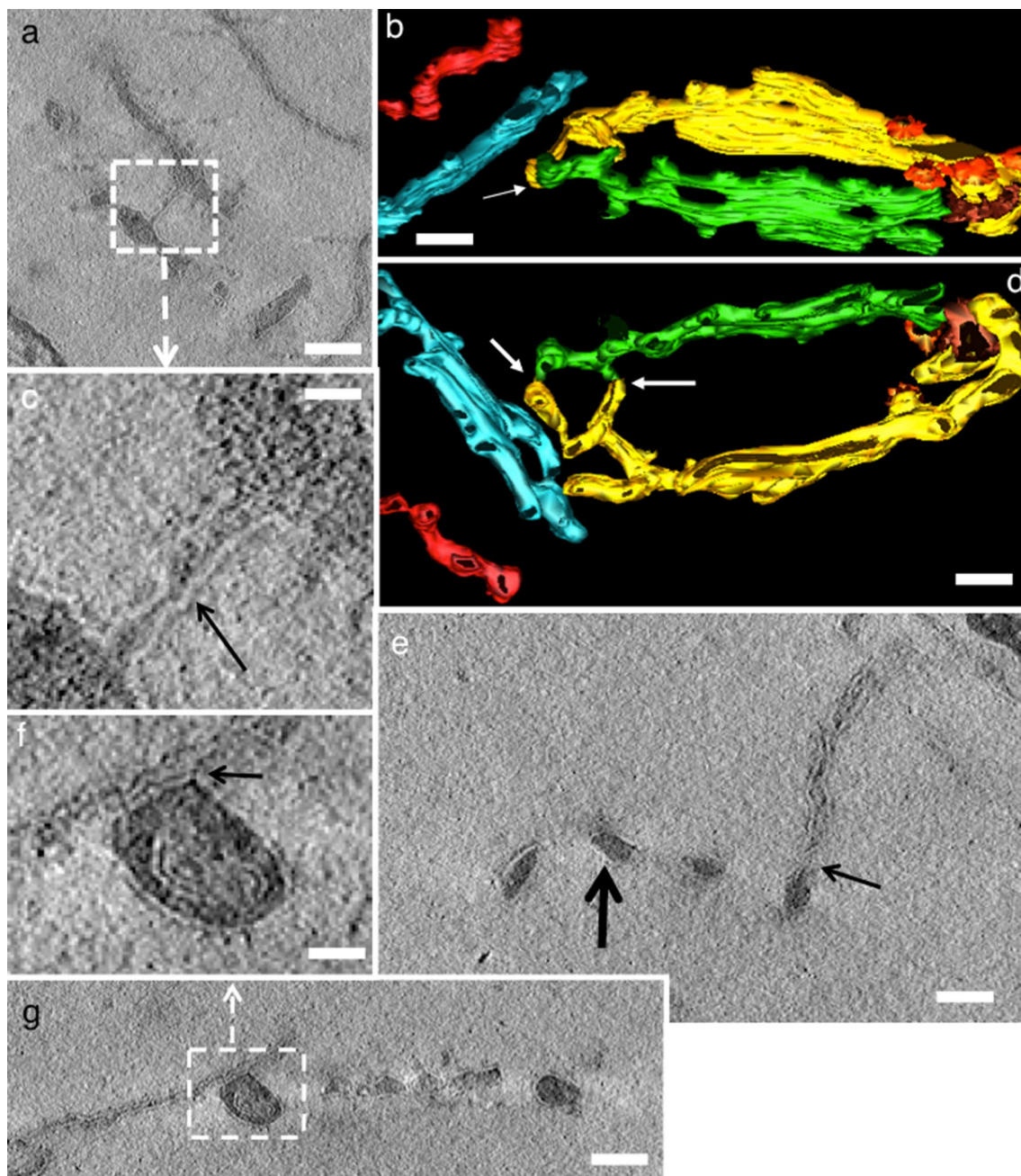
Fig. 5 Connections between different Golgi compartments. **a** Virtual tomography section showing membrane connections between medial (*upper*) and trans-Golgi compartment. **c** Higher magnification of the zone within the *white box* in **a**. **b**, **d** Membrane connections between the medial (*yellow*) and cis (*green*)-Golgi compartments are shown. Two different views of a 3D model obtained during rotation. The *white arrows* indicate thin tubules connecting two compartments. **e** Membrane continuity between the cis-Golgi compartment (*thick arrow*) and the ERES (*thin arrow*). Virtual tomography section (OTO method). **f**, **g** Contact of membranes (*black arrow* in **f**) without their fusion between the cis-Golgi compartment (to the right in **g**) and the ER. **f** is a magnification of the *white box* in **g**. *Scale bars* 120 nm panel **a**; 60 nm panels **b**, **d**, **f**, **g**; 30 nm panels **c**, **e**

Discussion

In the current paper, using improved protocols of sample preparation and immune labeling, we examined structures of ER, ERES, Golgi compartments, and vesicles in *S. cerevisiae*.

In the cytoplasmic sheet of the ER, we found narrow pores and aggregates of narrow pores near the rims. We also observed tubular networks tightly interconnected with sheets of several cytoplasmic ER cisternae. Similar observations have been made by others (Mari et al. 2014).

Within the Golgi compartments, we found disks with wide pores, disks with narrow pores and network-like structures with varicosities at the point of branching. On occasion, the Golgi disks appeared as deflated balls or semi-spheres. The lumen of these Golgi compartments was more osmiophilic than the lumen of the ER. In contrast to ER elements, all Golgi structures were isolated. Only the disks with wide pores were observed to be connected, albeit rarely, with the ER. These pores may form after fusion of the rims of the ER, and their concentration near the rims might form ERES that then fuse, or form, the cis-Golgi (Okamoto et al. 2012). According to the mechanism of transmembrane area asymmetry (Beznoussenko and Mironov 2015), the formation of COPI vesicles and buds could transform cis-networks into disks with narrow pores.

The vesicles with a diameter of 35–40 nm, whose number was fourfold lower than the number of 45–50 nm vesicles (Table S1), appear to be derived from clathrin-coated buds on the trans-Golgi. There are several lines of evidence supporting this: (1) Some of the 35–40 nm vesicles were partially coated with a clathrin-like coat; (2) the diameter of clathrin-coated buds on the trans-Golgi, and these vesicles are almost the same; (3) clathrin-dependent vesicles isolated from *S. cerevisiae* have a diameter after uncoating of 43 nm (Mueller and Branton 1984); (4) the size of clathrin-dependent vesicles derived from the PM appears to be about 40 nm (Kukulski et al. 2011, 2012a; Mari et al. 2014), in agreement with the description of endocytosis from the PM in yeast (Kukulski et al. 2012b). Our methods better visualize membranes so we observed significantly more vesicles in the yeast cytoplasm than in previous works (Morin-Ganet et al. 2000; Rambourg et al. 2001; West et al. 2011). Finally, we observed 55–90 nm vesicles with the well-known characteristics of secretory granules.

The second type of vesicle (45–50 nm) probably represents COPI-dependent vesicles. These vesicles were enriched for Gos1p and depleted for Rer1p. This observation fits well with the data reported by Fusella et al. (2013) where it was shown that GOS28 (GS28) and membrin (GS27), both Qb SNAREs, are enriched in COPI vesicles, and that these might be used for deceleration of intra-Golgi transport. This is also of interest in light of the description of different subtypes of COPI vesicles in plant and algal cells known as COPIa, which have been proposed to be confined to the ER–Golgi interface, and COPIb, which surround the medial and trans-Golgi cisternae, and reports of different COPI vesicle subtypes in mammalian cells (Day et al. 2013 and references therein).

We could not find any vesicles labeled with the COPII component Sec31p. To date, there has been no description of free COPII vesicles in *S. cerevisiae* in electron micrographs (this study; Preuss et al. 1991; Morin-Ganet et al. 2000; West et al. 2011; Mari et al. 2014; Papanikou et al. 2015). Using extremely high-speed and high-resolution confocal microscopy, Kurokawa et al. (2014) showed that the yeast cis-Golgi contacts the ERES, the COPII coat cage then collapses, and cargo is released into the cis-Golgi in what they describe as a hug-and-kiss action. Interestingly, we found connections between the ER and the cis-Golgi. While all of these data do not rule out the possibility that free COPII vesicles are released, but if so, they would argue that they are very short-lived entities. Live-cell fluorescence analysis of Golgi maturation (Matsuura-Tokita et al. 2006; Losev et al. 2006) showed that when the proximal compartment acquires the marker of the distal compartment, these two compartments are close to each other and there appear to be tubular connections between different Golgi compartments (Nakano and Luini 2010).

The morphological and immune-EM analyses indicate that Golgi disks with wide pores are cis-Golgi compartments, whereas disks with narrow pores are medial Golgi compartments, which was corroborated by CLEM analysis. Finally, networks with nodules and clathrin-coated buds probably represent trans-Golgi compartments.

On the other hand, our data should be evaluated from the point of view of existing models of intracellular transport. Currently, the two models of intra-Golgi transport that seem to be most widely accepted are the cisternal maturation model (Mironov et al. 1997, 1998; Bonfanti et al. 1998) and the kiss-and-run model (KARM; Mironov and Beznoussenko 2012; Mironov et al. 2013). The observation of connections between different Golgi compartments and between the ER and the cis-Golgi compartment made KARM suitable also for S. cerevisiae. Tubular continuities across Golgi sub-compartments have been also observed in mammalian cells (Marsh et al. 2004; Trucco et al. 2004; Beznoussenko et al. 2014). However, additional experiments are necessary in order to discover which model is more powerful.

Compliance with ethical standards

Conflict of interest The authors declare no conflict of interest.

References

Baharaeen S, Vishniac HS (1982) A fixation method for visualization of yeast ultrastructure in the electron microscope. Mycopathologia 77:19–22

Banta LM, Robinson JS, Klionsky DJ, Emr SD (1988) Organelle assembly in yeast: characterization of yeast mutants defective in vacuolar biogenesis and protein sorting. J Cell Biol 107:1369–1383

Barlowe C, Orci L, Yeung T, Hosobuchi M, Hamamoto S, Salama N, Rexach MF, Ravazzola M, Amherdt M, Schekman R (1994) COPII: a membrane coat formed by sec proteins that drive vesicle budding from the endoplasmic reticulum. Cell 77:895–907

Bednarek SY, Ravazzola M, Hosobuchi M, Amherdt M, Perrelet A, Schekman R, Orci L (1995) COPI– and COPII–coated vesicles bud directly from the endoplasmic reticulum in yeast. Cell 83:1183–1196

Beznoussenko GV, Mironov AA (2015) Correlative video–light–electron microscopy of mobile organelles. Methods Mol Biol 1270:321–346

Beznoussenko GV, Dolgikh VV, Seliverstova EV, Semenov PB, Tokarev YS, Trucco A, Micaroni M, Di Giandomenico D, Auinger P, Senderskiy IV, Skarlato SO, Snigirevskaya ES, Komissarchik YY, Pavelka M, De Matteis MA, Luini A, Sokolova YY, Mironov AA (2007) Analogs of the Golgi complex in microsporidia: structure and avesicular mechanisms of function. J Cell Sci 120:1288–1298

Beznoussenko GV, Parashuraman S, Rizzo R, Polishchuk R, Martella O, Di Giandomenico D, Fusella A, Spaar A, Sallese M, Capestrano MG, Pavelka M, Vos MR, Rikers YG, Helms V, Mironov AA, Luini A (2014) Transport of soluble proteins through the Golgi occurs by diffusion via continuities across cisternae. Elife. doi:10.7554/eLife.02009

Bonfanti L, Mironov AA Jr, Martínez-Menárguez JA, Martella O, Fusella A, Baldassarre M, Buccione R, Geuze HJ, Mironov AA, Luini A (1998) Procollagen traverses the Golgi stack without leaving the lumen of cisternae: evidence for cisternal maturation. Cell 95:993–1003

Castillon GA, Watanabe R, Taylor M, Schwabe TM, Riezman H (2009) Concentration of GPI-anchored proteins upon ER exit in yeast. Traffic 10:186–200

Day KJ, Staehelin LA, Glick BS (2013) A three-stage model of Golgi structure and function. Histochem Cell Biol 140:239–249

Fusella A, Micaroni M, Di Giandomenico D, Mironov AA, Beznoussenko GV (2013) Segregation of the Qb–SNAREs GS27 and GS28 into Golgi vesicles regulates intra–Golgi transport. Traffic 14:568–584

Geissinger HD, Vriend RA, Meade LD, Ackerley CA, Bhatnagar MK (1983) Osmium–thiocarbohydrazide–osmium versus tannic acid-osmium staining of skeletal muscle for scanning electron microscopy and correlative microscopy. Trans Am Microsc Soc 102:390–398

Glick BS, Luini A (2011) Models for Golgi traffic: a critical assessment. Cold Spring Harb Perspect Biol 3:a005215

Hawes C (2012) The ER/Golgi interface–is there anything in-between? Front Plant Sci 3:73

Hohenberg H, Mannweiler K, Müller M (1994) High-pressure freezing of cell suspensions in cellulose capillary tubes. J Microsc 175(Pt 1):34–43

Kang BH, Staehelin LA (2008) ER–to–Golgi transport by COPII vesicles in arabidopsis involves a ribosome–excluding scaffold that is transferred with the vesicles to the Golgi matrix. Protoplasma 234:51–64

Kolpakov V, Polishchuk R, Bannykh S, Rekhter M, Solovjev P, Romanov YE, Tararak E, Antonov A, Mironov A (1996) Atherosclerosis prone branch regions in human aorta: microarchitecture and cell composition of intima. Atherosclerosis 122:173–187

Koster AJ, Grimm R, Typke D, Hegerl R, Stoschek A, Walz J, Baumeister W (1997) Perspectives of molecular and cellular electron tomography. J Struct Biol 120:276–308

Kreft ME, Di Giandomenico D, Beznoussenko GV, Resnik N, Mironov AA, Jezernik K (2010) Golgi apparatus fragmentation as a mechanism responsible for uniform delivery of uroplakins to the apical plasma membrane of uroepithelial cells. Biol Cell 102:593–607

Kremer JR, Mastronarde DN, McIntosh JR (1996) Computer visualization of three–dimensional image data using IMOD. J Struct Biol 116:71–76

Kukulski W, Schorb M, Welsch S, Picco A, Kaksonen M, Briggs JA (2011) Correlated fluorescence and 3D electron microscopy with high sensitivity and spatial precision. J Cell Biol 192:111–119

Kukulski W, Schorb M, Welsch S, Picco A, Kaksonen M, Briggs JA (2012a) Precise, correlated fluorescence microscopy and electron tomography of lowicryl sections using fluorescent fiducial markers. Methods Cell Biol 111:235–257

Kukulski W, Schorb M, Kaksonen M, Briggs JA (2012b) Plasma membrane reshaping during endocytosis is revealed by time–resolved electron tomography. Cell 150:508–520

Kurokawa K, Okamoto M, Nakano A (2014) Contact of cis–Golgi with ER exit sites executes cargo capture and delivery from the ER. Nat Commun 5:3653. doi:10.1038/ncomms4653

Levi SK, Bhattacharyya D, Strack RL, Austin JR 2nd, Glick BS (2010) The yeast GRASP Grh1 colocalizes with COPII and is dispensable for organizing the secretory pathway. Traffic 11:1168–1179

Losev E, Reinke CA, Jellen J, Strongin DE, Bevis BJ, Glick BS (2006) Golgi maturation visualized in living yeast. Nature 441:1002–1006

Luft JH (1961) Improvements in epoxy resin embedding methods. J Biophys Biochem Cytol 9:409–414

Mari M, Geerts WJ, Reggiori F (2014) Immuno– and correlative light microscopy–electron tomography methods for 3D protein localization in yeast. Traffic 15:1164–1178

Marsh BJ, Volkmann N, McIntosh JR, Howell KE (2004) Direct continuities between cisternae at different levels of the Golgi complex in glucose–stimulated mouse islet beta cells. Proc Natl Acad Sci USA 101:5565–5570

Mastronarde DN (2005) Automated electron microscope tomography using robust prediction of specimen movements. J Struct Biol 152:36–51

Matsuura-Tokita K, Takeuchi M, Ichihara A, Mikuriya K, Nakano A (2006) Live imaging of yeast Golgi cisternal maturation. Nature 441:1007–1010

McNew JA, Coe JG, Søgaard M, Zemelman BV, Wimmer C, Hong W, Söllner TH (1998) Gos1p, a Saccharomyces cerevisiae SNARE protein involved in Golgi transport. FEBS Lett 435:89–95

Micaroni M, Perinetti G, Di Giandomenico D, Bianchi K, Spaar A, Mironov AA (2010) Synchronous intra–Golgi transport induces the release of Ca2 + from the Golgi apparatus. Exp Cell Res 316:2071–2086

Mironov AA, Beznoussenko GV (2012) The kiss–and–run model of intra–Golgi transport. Int J Mol Sci 13:6800–6819

Mironov AA Jr, Mironov AA (1998) Estimation of subcellular organelle volume from ultrathin sections through centrioles with a discretized version of vertical rotator. J Microsc 192:29–36

Mironov AA, Weidman P, Luini A (1997) Variations on the intracellular transport theme: maturing cisternae and trafficking tubules. J Cell Biol 138:481–484

Mironov A Jr, Luini A, Mironov A (1998) A synthetic model of intra-Golgi traffic. FASEB J 12:249–252

Mironov AA, Colanzi A, Polishchuk RS, Beznoussenko GV, Mironov AA Jr, Fusella A, Di Tullio G, Silletta MG, Corda D, De Matteis MA, Luini A (2004) Dicumarol, an inhibitor of ADP–ribosylation of CtBP3/BARS, fragments Golgi non–compact tubular zones and inhibits intra–Golgi transport. Eur J Cell Biol 83:263–279

Mironov AA, Sesorova IV, Beznoussenko GV (2013) Golgi's way: a long path toward the new paradigm of the intra–Golgi transport. Histochem Cell Biol 140:383–393

Morin-Ganet MN, Rambourg A, Deitz SB, Franzusoff A, Kepes F (2000) Morphogenesis and dynamics of the yeast Golgi apparatus. Traffic 1:56–68

Mueller SC, Branton D (1984) Identification of coated vesicles in Saccharomyces cerevisiae. J Cell Biol 98(1):341–346

Nakano A, Luini A (2010) Passage through the Golgi. Curr Opin Cell Biol 22:471–478

Okamoto M, Kurokawa K, Matsuura-Tokita K, Saito C, Hirata R, Nakano A (2012) High curvature domains of the ER are important for the organization of ER exit sites in Saccharomyces cerevisiae. J Cell Sci 125:3412–3420

O'Toole ET, Winey M, McIntosh JR, Mastronarde DN (2002) Electron tomography of yeast cells. Methods Enzymol 351:81–95

Papanikou E, Glick BS (2009) The yeast Golgi apparatus: insights and mysteries. FEBS Lett 583:3746–3751

Papanikou E, Day KJ, Austin J, Glick BS (2015) COPI selectively drives maturation of the early Golgi. Elife. doi:10.7554/eLife.13232

Polishchuk RS, Mironov AA (2004) Structural aspects of Golgi function. Cell Mol Life Sci 61:146–158

Polishchuk RS, Polishchuk EV, Mironov AA (1999) Coalescence of Golgi fragments in microtubule–deprived living cells. Eur J Cell Biol 78:170–185

Preuss D, Mulholland J, Kaiser CA, Orlean P, Albright C, Rose MD, Robbins PW, Botstein D (1991) Structure of the yeast endoplasmic reticulum: localization of ER proteins using immunofluorescence and immunoelectron microscopy. Yeast 7:891–911

Preuss D, Mulholland J, Franzusoff A, Segev N, Botstein D (1992) Characterization of the Saccharomyces Golgi complex through the cell cycle by immunoelectron microscopy. Mol Biol Cell 3:789–803

Rambourg A, Clermont Y, Kepes F (1993) Modulation of the Golgi apparatus in Sacharomyces cerevisiae sec7 mutants as seen by three–dimensional electron microscopy. Anat Rec 237:441–452

Rambourg A, Clermont Y, Ovtracht L, Képès F (1995) Three-dimensional structure of tubular networks, presumably Golgi in nature, in various yeast strains: a comparative study. Anat Rec 243:283–293

Rambourg A, Jackson CL, Clermont Y (2001) Three dimensional configuration of the secretory pathway and segregation of secretion granules in the yeast Saccharomyces cerevisiae. J Cell Sci 114:2231–2239

Rossanese OW, Soderholm J, Bevis BJ, Sears IB, O'Connor J, Williamson EK, Glick BS (1999) Golgi structure correlates with transitional endoplasmic reticulum organization in Pichia pastoris and Saccharomyces cerevisiae. J Cell Biol 145:69–81

Ryan US, Hart MA (1986) Electron microscopy of endothelial cells in culture: II. scanning electron microscopy and OTOTO impregnation method. J Tissue Cult Methods 10:35–36

Sato K, Sato M, Nakano A (2001) Rer1p, a retrieval receptor for endoplasmic reticulum membrane proteins, is dynamically localized to the Golgi apparatus by coatomer. J Cell Biol 152:935–944

Shindiapina P, Barlowe C (2010) Requirements for transitional endoplasmic reticulum site structure and function in Saccharomyces cerevisiae. Mol Biol Cell 21:1530–1545

Trucco A, Polishchuk RS, Martella O, Di Pentima A, Fusella A, Di Giandomenico D, San Pietro E, Beznoussenko GV, Polishchuk EV, Baldassarre M, Buccione R, Geerts WJ, Koster AJ, Burger KN, Mironov AA, Luini A (2004) Secretory traffic triggers the formation of tubular continuities across Golgi sub–compartments. Nat Cell Biol 6:1071–1081

Vanhecke D, Studer L, Studer D (2007) Cryoultramicrotomy: cryoelectron microscopy of vitreous sections. Methods Mol Biol 369:175–197

Walther P, Ziegler A (2002) Freeze substitution of high–pressure frozen samples: the visibility of biological membranes is improved when the substitution medium contains water. J Microsc 208:3–10

Weigert R, Colanzi A, Mironov A, Buccione R, Cericola C, Sciulli MG, Santini G, Flati S, Fusella A, Donaldson JG, Di Girolamo M, Corda D, De Matteis MA, Luini A (1997) Characterization of chemical inhibitors of brefeldin a–activated mono–ADP–ribosylation. J Biol Chem 272:14200–14207

West M, Zurek N, Hoenger A, Voeltz GK (2011) A 3D analysis of yeast ER structure reveals how ER domains are organized by membrane curvature. J Cell Biol 193:333–346

Wright R (2000) Transmission electron microscopy of yeast. Microsc Res Tech 51:496–510